Interpretation of recent alpine landscape system evolution using geomorphic mapping and L-band InSAR analyses

メタデータ	言語: eng 出版者: 公開日: 2019-01-15 キーワード (Ja): キーワード (En): 作成者: Imaizumi, Fumitoshi, Nishiguchi, Takaki, Matsuoka, Norikazu, Trappmann, Daniel, Stoffel, Markus メールアドレス: 所属:
URL	http://hdl.handle.net/10297/00026247

Interpretation of recent alpine landscape system evolution using geomorphic mapping and L-band InSAR analyses

Fumitoshi Imaizumi[a], Takaki Nishiguchi[b], Norikazu Matsuoka[c], Daniel Trappmann[d, e], Markus Stoffel[d, f, g]

a Faculty of Agriculture, Shizuoka University
836 Ohya, Suruga, Shizuoka 422-8529, Japan

b NIPPON KOEI CO., LTD.
1-14-6 Kudankita, Chiyoda-ku Tokyo, 102-0073, Japan

c Faculty of Life and Environmental Sciences, University of Tsukuba
1-1-1 Ten-noudai, Tsukuba, Ibaraki 305-8572, Japan

d Climate Change Impacts and Risks in the Anthropocene (C-CIA), Institute for Environmental Sciences, University of Geneva, 66 Boulevard Carl-Vogt, CH-1205 Geneva, Switzerland

e Bayerische Landesanstalt für Wald und Forstwirtschaft
Abt. 3 Waldbau und Bergwald, Hans-Carl-von-Carlowitz-Platz 1, 85354 Freising, Germany

f Dendrolab.ch, Department of Earth Sciences, University of Geneva, 13 rue des Maraîchers, CH-1205 Geneva, Switzerland

g Department F.-A. Forel for Aquatic and Environmental Sciences, University of Geneva, 66 Boulevard Carl-Vogt, CH-1205 Geneva, Switzerland

Abstract

Alpine landscapes are typically characterized by inherited features of past glaciations and, for the more recent past, by the interplay of a multitude of types of geomorphic processes, including permafrost creep, rockfalls, debris flows, and landslides. These different processes usually exhibit large spatial and temporal variations in activity and velocity. The understanding of these processes in a wide alpine area is often hindered by difficulties in their surveying. In this study, we attempt to disentangle recent changes in an alpine landscape system using geomorphic mapping and L-band DInSAR analyses (ALOS-PALSAR) in the Zermatt Valley, Swiss Alps. Geomorphic mapping points to a preferential distribution of rock glaciers on north-facing slopes, whereas talus slopes are concentrated on south-facing slopes. Field-based interpretation of ground deformation in rock glaciers and movements in talus slopes correlates well with the ratio of InSAR images showing potential ground deformation. Moraines formed during the Little Ice Age, rock glaciers, and talus slopes on north-facing slopes are more active than landforms on south-facing slopes, implying that the presence of permafrost facilitates the deformation of these geomorphic units. Such deformations of geomorphic units prevail also at the elevation of glacier termini. For rock cliffs, the ratio of images indicating retreat is affected by slope orientation and elevation. Linkages between sediment supply from rock cliffs and sediment transport in torrents are different amongst tributaries, affected by relative locations between sediment supply areas and the channel network. We conclude that the combined use of field surveys and L-band DInSAR analyses can substantially improve process understanding in steep, high-mountain terrain.

Key words: InSAR analyses; geomorphic mapping; alpine landscape; rock glacier

1. Introduction

Alpine landscapes are constantly shaped by a multitude of geomorphic processes with largely differing spatial and temporal activity, such as rockfalls, floods, permafrost creep, debris flows, or landslides (e.g., Haeberli et al., 2006; Korup et al., 2010; Lugon and Stoffel, 2010; Schneuwly-Bollschweiler and Stoffel, 2012; Barboux et al., 2014). Understanding their rates and patterns of activity is usually restricted to field surveys at individual sites, such that studies focusing on larger surface areas have remained relatively scarce. In the past, geomorphic mapping has been based widely on aerial photograph interpretations, analyses of airborne LiDAR (light detection and ranging) data, and field surveys to interpret types of processes occurring in alpine environments (e.g., Ikeda and Matsuoka, 2002; Lugon et al., 2004; Otto et al., 2009). However, and because present landscapes are a result of current and past geomorphic processes, detection of current process activity is often limited in cases where interpretation relies on geomorphic mapping alone. On the other hand, field monitoring and periodical LiDAR surveys provide quantitative data on current geomorphic activity but also require substantial labor and budgets.

The Interferometric Synthetic Aperture Radar (InSAR), by contrast, can be used to detect small deformations of the ground surface (in the order of millimeter to centimeter) and has been used in recent years for the detection of activity of volcanic (Lu et al., 2010; Schaefer et al., 2015), rockfall (Arosio et al., 2009; Rouyet et al., 2017), landslide (Peyret et al., 2008; Jebur et al., 2014; Singleton et al., 2014; Nishiguchi et al., 2017), and rock glacier (Liu et al., 2013; Barboux et al., 2014) processes. Recent results are promising, and the approach is thought to greatly improve understanding of geomorphic systems in alpine environments.

The choice of sensors and analysis methods in InSAR-based studies is typically based on land cover, characteristics of the geomorphic processes, and available data. For example, ground based InSAR (GB-InSAR) is frequently used for the detection of rockfall activity in fairly small areas (Arosio et al., 2009; Rouyet et al., 2017) because rockfall source areas are usually on subvertical slopes in which space-borne InSAR analyses repeatedly fail because of the problem of layover (Bamler and Hartl, 1998). In contrast, space-borne SAR images are usually used for the detection of ground surface deformation in those areas where topography is more gentle (Saroli et al., 2005; Liu et al., 2010). Permanent Scatter Interferometric Synthetic Aperture Radars (PSInSAR) are usually employed in areas with artificial structures (Strzelczyk et al., 2009), as the latter can be used as stable radar targets (or as so-called PS points). Finally, differential InSAR (DInSAR) approaches using L-band images are applicable in those areas covered by deep forests, lacking artificial structures that could be used as PS points (Roering et al., 2009; Barboux et al., 2014; Nishiguchi et al., 2017).

Interestingly, a large array of published work focused on a very specific geomorphic process, such that only very few studies have attempted to understand entire geomorphic systems by single InSAR analysis so far (Barboux et al., 2014). As a consequence, a clear need exists for analytical procedures that are able to detect activity of various mass transfer processes and therefore can enhance our understanding of larger, and often complex, geomorphic systems.

The data used in this study was generated by a phased array type L-band Synthetic Aperture Radar (PALSAR), which was mounted on the Advanced Land Observing Satellite (ALOS). The device is classified as an L-band SAR and was launched on 24 January 2006. The wavelength of PALSAR is longer than the X-band radar (typified by COSMO-SkyMed and TerraSAR-X) and the C-band radar (typified by Envisat and RADARSAT-2), which have been widely used in Europe and North America in the past. Although the resolution of the X- and C-band SARs are higher than that of the L-band SAR, PSInSAR, a widely used technique for the analysis of X- and C-band SAR images, requires PS points (Strzelczyk et al., 2009; Oliveira et al., 2015). Therefore, any DInSAR analyses using PALSAR images will have clear advantages in the detection of any ground surface deformation in areas lacking artificial structures (Strozzi et al., 2005; Roering et al., 2009). In addition, coherence of InSAR analysis using short wavelength images (i.e., C-band SAR) has been demonstrated to be generally low for long observation periods (>100 days) between images, mainly because of changes in ground surface conditions (Zebker and Villasenor, 1992). By contrast, past studies based on L-band SAR have shown clearly that image pairs with longer observation periods can be used without major problems (Wei and Sandwell, 2010; García-Davalillo et al., 2014) and that L-band SAR seems ideal for the detection of moderate ground surface deformations (Nishiguchi et al., 2017).

The purpose of this paper is to understand geomorphic process activity and changes over time in an alpine high-relief landscape system of the Swiss Alps by coupling field-based geomorphic mapping with L-band DInSAR analysis based on PALSAR images. The DInSAR analysis was used to interpret the spatial variability of geomorphic processes over a wide alpine area, which is too large to be covered by field surveys alone. Results of DInSAR analysis were cross-validated by field surveys in order to avoid misinterpretation affected by topography, atmosphere, and noise (Roering et al., 2009; García-Davalillo et al., 2014). By doing so, we interpret recent activity of various types of geomorphic processes, including movements of rock glaciers, rockfalls, landslides, and deformation of talus slopes and moraines, in the Zermatt Valley (also referred to in the literature as Mattertal or Matter Valley). We selected ALOS/PALSAR material rather than images from the currently working sensors (e.g., ALOS-2/PALSAR-2). This choice was motivated by the fact that the number of image pairs observed by the new L-band sensors is not yet large enough for the analyses of geomorphic processes in the study area. Although ALOS has already retired, our findings using PALSAR images are considered to be beneficial for the analysis of other L-band sensors as well.

2. Study area

The study was conducted on the east-facing slopes of the Zermatt Valley, a very deep and narrow glaciated valley; the study area is located in the southern Swiss Alps and is 10 km wide and 3 km deep and has a surface of 99 km^2 (Fig. 1). Geomorphology in the Zermatt Valley is characterized by a large array of mass transfer processes, including permafrost creep (Lugon and Stoffel, 2010; Wirz et al., 2016), rockfalls (Stoffel et al., 2005), landslides and rockslides (Willenberg et al., 2008b; Stoffel and Huggel, 2012), and debris flows (e.g., Bollschweiler and Stoffel, 2010; Schneuwly-Bollschweiler and Stoffel, 2012; Stoffel et al., 2014). The basement rock in this area, mainly Permian gneiss and quartzite, is hard when intact but becomes highly deformed and fractured by folding, gravitational creep, and periglacial processes (Willenberg et al., 2008b).

The western tributaries of the Mattervispa River cut the steep slopes of the Zermatt Valley and are aligned in a north-south direction in the study area. Above treeline, locally at about 2200 m asl, alpine grasslands spread over previously glaciated, gentle terrains between 2400 to 2600 m asl and are surrounded by steep and high mountains, the summits of which range from 3100 to 4505 m asl (Fig. 1B). Many of the slopes underneath these summits are underlain by permafrost (Gruber and Hoelzle, 2001). Rock glaciers and talus slopes, composed of rock debris derived from outcrops of these mountains, are distributed near the boundaries between these high mountains and the gentle terrains (Fig. 1B). Vegetation cover is very limited on mountains and on most of the rock glaciers and talus slopes. Glaciers are widespread at the highest elevations of the large tributaries (>2800 m asl) but have retreated significantly since the end of the Little Ice Age (LIA) around 1850 CE (Joerin et al., 2006).

Sub-vertical, glaciated rock cliffs (40°–80°) are exposed at elevations ranging from 1000 to 2400 m asl along the Mattervispa River (Fig. 1C). In April and May 1991, a series of rockslides with a total volume of 30 million m^3 severely altered the landscape around Randa (Willenberg et al., 2008a, 2008b). A number of smaller slope failures (with areas <10,000 m^2) have occurred on other rock cliffs. Between these rock cliffs, conifer trees grow in tiny flat spaces. Farther down, debris flow fans occur at the confluence of tributaries with the Mattervispa River, whereas talus slopes can be found mostly at the base of rock cliffs.

On the sparsely wooded surfaces around 1800 m asl, annual average precipitation is estimated to be 660 mm (Stoffel et al., 2005). Precipitation is highest between August and November when persistent rain from low-pressure masses in the Mediterranean Sea may penetrate into this inner-alpine valley. At elevations above 2400 m asl, snow usually covers the slope from autumn to spring. Snow covers some portion of the study area above 2900 m asl even in summer, especially on north-facing slopes (where avalanche deposits may sometimes persist for several years). Snow accumulation is much more limited on the steep rock cliffs at elevations of 1000 to 2400 m asl, even in winter. Mean annual air temperature in Zermatt (1638 m asl), 18 km south of St. Niklaus, is 3.9°C (1900–2008) (Stoffel et al., 2013). Using a temperature lapse rate of 5°C km^{-1}, mean annual air temperature at 2400 m asl is estimated to be -0.1°C.

3. Material and methods

3.1. Mapping of geomorphic units

The spatial distribution of seven major geomorphic units was mapped in a geographical information system (GIS) using digital ortho photos from 2005 with a grid size of 0.5 m, stereo photo pairs from 2005 at a scale ranging from 1:20,000 to 1:30,000, and with information contained in the online topographic map (map.geo.admin.ch) at a scale of 1:25,000, updated in 2017 (Table 1). Slope gradients were calculated from the digital elevation model DHM25 (swisstopo) at 25-m resolution and used as another source of information for the classification of geomorphic units. Mapping was based primarily on surface topography of geomorphic units and their location relative to hillslopes and channels. This also means that debris-covered glaciers were not added to glaciers in this study because we mapped glaciers visually based on visible ice on aerial photographs and satellite imagery. Because the aerial photographs used in this study (taken in 2005) are three to four years older than that of the satellite imagery of the same study zone and 11 years older than the field surveys in 2016, we also checked temporal changes in the spatial distribution of geomorphic units in Google Earth. A comparison between our geomorphic map and Google Earth shows that changes in the spatial distribution of geomorphic units in most cases are very minor or not evident over the last 11 years, except for the recession of glaciers. Topographic attributes for each geomorphic unit, including slope angle, slope direction, and average elevation, were calculated by the GIS software QGIS on the basis of the DHM25 DEM available from swisstopo.

3.2. InSAR analysis

In this study, we used PALSAR L-band SAR data laid over ALOS (Table 2) with an observation width, resolution, and off-nadir angle of 40–70 km, 14–88 m, and 34.3° respectively. Because most parts of the study area are facing either east or southeast, we used images with ascending orbit direction (right looking). Calculation of SAR interferometry images was performed with RINC (Ver. 0.36), a software developed by the National Research Institute for Earth Science and Disaster Prevention (Ozawa et al., 2016). To remove the topographic phase, we used the 30-m-grid digital ellipsoidal height model (DEHM) created by the Shuttle Radar Topography Mission 1 (SRTM-1). The interferometry images with radar coordinate systems were divided into small sections and projected to geographic coordinate systems by offset and affine transformations of each section. All of the study area was covered by one interferometry image. For the unwrapping, the Statistical-cost, Network-flow Algorithm for Phase Unwrapping (SNAPHU) (Chen and Zebker, 2002) was applied by using the minimum spanning tree (MST) algorithm (Graham and Hell, 1985). Phase difference obtained by phase unwrapping was converted to displacement along the slant range direction by using the following equation: $\lambda / 4\pi$, where λ is the wavelength of PALSAR (236 mm). Following this, the stable area was assigned a displacement of 0 mm, with the values extending from the center point to generate the scale used in the displacement maps. We used maps showing the displacement to detect potential deformation areas. Areas with multiple pixels (generally wider than six pixels) and with markedly different displacements from the surrounding areas on the displacement map were extracted as potential deformation areas. At the same stage, we excluded areas with obvious noise (e.g., foreshortening, radar shadow, and layover) from the potential deformation areas. The ratio of images indicating potential ground deformation *n*, which was obtained by the number of image pairs indicating potential ground deformation in each geomorphic units divided by the total number of pairs (three in this study), was calculated for all geomorphic units *i* as an indicator of activity of geomorphic processes as interpreted by InSAR analysis. We also calculated coherence, defined here as the absolute value of normalized complex correlation coefficient between two images (Wegmuller and Werner, 1995), using RINC in order to discuss reliability of analyses.

Three PALSAR image pairs with high coherence were then selected for the analyses (Table 2). The selection of images was restricted to summer and autumn in order to have the smallest possible extent of snow cover in the study area. The duration between two image pairs in periods 2 and 3 (46 days) are shorter than in period 1 (368 days). All periods include imagery taken in summer and/or autumn when activity of rock glaciers is usually highest in the study area (Delaloye et al., 2010; Fischer et al., 2012).

3.3. Field surveys

Results of the InSAR analyses were validated by field surveys undertaken in the validation area, composed of the Embdbach and Jungbach catchments (in the northern part of the study area) in early August 2016 (Fig. 1). These catchments were selected for field surveys as all major geomorphic units in the Zermatt Valley (i.e., rock glacier, talus slope, rock cliff, glacier, moraine, landslide, debris flow cone) are present within a small area. Geomorphic activity at 16 rock glaciers and 11 talus slopes was classified into three groups (inactive, active, very active) based on the presence and state of vegetation, lichens, and regolith (Table 3), as their abundance and/or absence can be attributed to different degrees of process activity (Hamilton and Whalley, 1995; Ikeda and Matsuoka, 2002; Burga et al., 2004). Activity of rock glaciers was also interpreted by the steepness of the front and the presence of wrinkles and cracks on the rock glacier surface (Ikeda and Matsuoka, 2002; Berger et al., 2004; Roer et al., 2008). Activity of talus slopes was assessed by the presence of fresh clasts on its surface. Because activity of rock cliffs could not be directly interpreted by their appearance in the present case, activity of rock glaciers and talus slopes underneath 24 rock cliffs was compared with the interpretation of InSAR analyses. This combined approach allowed estimation of sediment supply from rock cliffs as controlling factors of the development of talus slopes and rock glaciers (Burger et al., 1999; Humlum, 2000) at the test sites. The activity of a rock cliff fringed by multiple rock glaciers and talus slopes with different activities was represented by the highest activity among them. Activity of each geomorphic unit obtained by the field surveys were compared with ratio of InSAR images indicating potential ground deformation for the sake of validation of InSAR analysis.

4. Results

4.1. Spatial distribution of the geomorphic units

Geomorphic mapping of gravitational features shows that the rock cliffs in the study area are mostly along the western end of the study area (Fig. 2). In its northern part, rock glaciers and talus slopes are distributed primarily below rock cliffs (Fig. 2A). In the southern part, by contrast, slopes fringing rock cliffs are widely covered by glaciers and are thus lacking rock glaciers and talus slopes (Fig. 2B). Moraines formed during the LIA occur on both sides and in the frontal parts of the glaciers, whereas moraines formed during the Late Glacial (LG) period are at much lower elevations.

The geomorphic units also show a characteristic altitudinal distribution as illustrated in Fig. 3. That is, substantial ratios of the rock cliffs (96%) and glaciers (95%) are at higher elevations above 2750 m asl (Figs. 3D, 3E). Similarly, more than 90% of the rock glaciers are in the range from 2500 to 3000 m asl (Fig. 3B). Compared to the rock glaciers, talus slopes are mainly at similar or even slightly higher elevations (70% in the range from 2500 to 3250 m asl; Fig. 3C). The LIA moraines are, in most cases (88%), at elevations ranging from 2500 to 3000 m, whereas 90% of LG moraines are between 2250 and 2750 m asl (Fig. 3F). Landslide scars are restricted mostly to subvertical rock walls at elevations below 2250 m asl along the Mattervispa River (Fig. 3G). At elevations exceeding 2500 m asl, recent landslide scars are virtually nonexistent. Debris flow cones are found at the junctions of tributaries with the Mattervispa River; they are all at elevations below 1500 m asl (Fig. 3H).

A large proportion of the rock cliffs and glaciers face northeast, east, and southeast, which corresponds to the predominant slope directions over the entire study area (Figs. 4A, 4D, 4E). Southeast is also the dominant orientation for moraines (in LIA and LG) and debris flow cones, which again corresponds to the flow direction of tributaries (Figs. 4F, 4H). Slope directions of rock glaciers and talus slopes are nearly opposite (Figs. 4B and 4C). Many rock glaciers in the area are on the north-facing slopes, whereas talus slopes tend to occur on south-facing slopes. Most of the remaining talus slopes developed on north-facing slopes are in fact below or next to rock glaciers (distance <200 m).

4.2. InSAR analyses

InSAR analyses show that the number of image pairs displaying ground deformations varies between geomorphic units (Figs. 5, 6, 7). For example, deformations were detected in the case of rock glacier RG1 and talus slope TS1 in all three periods, whereas deformation was detected only in period 1 at rock glacier RG2 (Figs. 5, 6). Displacement and coherence in the case of glaciers (e.g., G1 and G2 in Fig. 5) is high and low respectively when compared with the surrounding areas; this is because of the active movement of the glacier. Displacement in LIA moraine is partly high in those areas nearby glaciers and active rock glaciers (e.g., at the southern end of M1 in Fig. 5). This finding is in line with the results of the field survey where the very limited recovery of lichens on only small patches testified high displacement at M1.

Ground deformation was detected in the scar of the Randa rockslide (LS2 in Fig. 7) and in the upper parts of those talus slopes formed by sediment from the rockslide (TS2 in Fig. 7A). During the field survey, recovery of vegetation was identified in the lower part of the talus slope, whereas almost no recovery was found in its upper part. This agrees with the result of the InSAR analysis detecting deformations in the upper part of the slope. Although exposure of fresh rock (i.e., light-colored surface without recovery of vegetation) can also be seen in the aerial photographs at landslide scars LS1 and LS3 (Fig. 7), deformation in these landslide scars was not detected by InSAR analyses. No clear changes were found in any of the debris flow cones in the three periods (e.g., DC1 and DC2 in Fig. 7). Interpretation using aerial photographs and Google Earth did not show any debris flow spilling out from channels during the study period. Displacement calculated by the InSAR analyses on the steep slopes around RC2 (slope gradient >60º) are spatially constant. Coherence on this slope is 0, indicating that the analyses failed because of the radar shadow.

Coherence in the geomorphic units depends above all on topographic factors (i.e., elevation, slope gradient) and the type of geomorphic units (Fig. 8). The glaciers show clearly lower coherence when compared to the other geomorphic units (Fig. 8A). As a result, coherence of the geomorphic units, with the exception of the rock cliffs and glaciers, ranges from 0.2 to 0.8 regardless of slope gradient (Fig. 8A). Coherence of the rock cliffs, by contrast, has a clear negative relationship with slope gradient ($R^2 = 0.35$, $p < 0.001$). The coherence of the geomorphic units in southeastern to southern directions, in which foreshortening hardly occurs in analyses if images from the ascending orbit are used, was higher than those in the northern to eastern directions (average 0.46, 0.33 respectively; Fig.

8B). We also realize that coherence is low at elevations from 1500 to 2000 m and above 3500 m asl, in which steep rock cliffs are dominant (Fig. 8C). Regardless of the type of geomorphic unit, coherence is also low at elevations ranging between 3000 and 3500 m asl, where snow partly covers the ground surface.

4.3. Validation of InSAR analyses

Activity of rock glaciers and talus cones was interpreted as being low at lower elevations (i.e., <2500 m asl) in the validation site (Fig. 6) based on visual assessment during field surveys. Rock glacier activity was classified as very active (activity 3) for all sites on north-facing slopes (Fig. 6). For the sake of comparison, the ratio of InSAR images indicating potential ground deformation n for rock glaciers and talus slopes in each field-based activity group (activities 1 to 3) was then interpreted using an average value to assess relationship between the ratio of images and the in situ activity (Table 4). For rock glaciers and talus slopes, the ratios of images showing potential deformation was clearly highest for those units that were rated as very active (3) during field surveys. By contrast, the ratio of images showing potential deformation in rock cliff areas had a weak relationship with the in situ activity of rock glacier and talus slopes located at the lower part of the rock cliffs. To exclude the unreliable results, the average ratio of images showing potential deformation was recalculated by using only the results of units with higher coherence (Table 5). We realize that differences in the ratio of images showing potential deformation between activity 1 (inactive) and activity 3 (very active) for rock cliffs were most significant when the threshold value of the coherence was set at 0.2. In addition, the ratio of images showing deformation on inactive talus slopes (activity 1) was zero at threshold coherence 0.2, implying that misdetection was prevented by removing low-coherence results. In this study, we thus consider a coherence of 0.2 as being a common threshold for a reliable assessment of geomorphic units.

4.4. Activity of geomorphic processes in the entire study area

In order to investigate the spatial extent of activity for each geomorphic unit in the entire study area, the average ratio of images showing ground deformation was calculated for each elevational class by using the following equation:

$$N_j = \frac{\sum_{i=1}^{k} n_i a_{i,j}}{\sum_{i=1}^{k} a_{i,j}} \quad (1)$$

where N_j is the average ratio of images showing deformation for the analyzed geomorphic type in elevation class jth, k is the number of geomorphic units classified as the analyzing geomorphic type, n_i is the ratio of images showing potential deformation in the area of geomorphic units ith, $a_{i,j}$ is the area of the geomorphic units ith covering the elevation class jth (Fig. 3). Geomorphic units with an average coherence of <0.20 were excluded from the analysis. For rock glaciers, the average ratio of images showing potential deformation shows a moderate peak of occurrence at elevations ranging from 2500 to 2750 m asl (Fig. 3B). Differences in the average ratio of images among elevation classes is insignificant for rock cliffs (Fig. 3D). By contrast, talus slopes show clearly that the ratio of images is higher at higher elevations (Fig. 3C). In the case of moraines formed during the LIA, the ratio of images showing deformation is clearly higher at elevations above 2500 m compared to lower elevations (Fig. 3F). Not surprisingly, no deformation could be found in LG moraines. For landslide scars, the average ratio of images showing ground deformation is high around the upper part of the subvertical slopes along the Mattervispa Valley at elevations ranging from 2000 to 2500 m asl (Fig. 3G). By contrast, no potential deformation was identified on the debris flow cones on InSAR images in all three pairs. In addition, decorrelation in InSAR analysis, which occurs when topography changes significantly during the observation period, was also not identified on debris flow cones. This agrees with the interpretations using aerial photographs and Google Earth.

Similarly, the average ratio of images showing potential deformation in the entire study area was calculated for each slope direction using the following equation:

$$M_l = \frac{\sum_{i=1}^{k} n_i a_{i,l}}{\sum_{i=1}^{k} a_{i,l}} \quad (2)$$

where M_l is the average ratio of images showing deformation for the analyzed geomorphic type at slope direction lth, $a_{i,l}$ is the area of geomorphic units ith covering slope direction lth (Fig. 4). Rock glaciers, talus slopes, and LIA moraines, which are all composed of rock debris, show clear trends for higher ratios for northern exposures when compared to southern exposures (Figs. 4B, 4C, 4F).

Although the ratio of images showing deformation in rock cliffs does not have a clear relationship with elevation and/or slope direction (Figs. 3D, 4D), some trends can be seen if both factors are analyzed together (Table 6). The ratio of images is high at lower elevations (i.e., <3000 m asl) in the case of north-facing rock cliff and also high at higher elevations (>3250 m asl) on south-facing cliffs.

5. Discussion

5.1. Availability of InSAR analyses for the interpretation of geomorphic processes

Displacement along the slant range direction was used here to successfully detect potential ground deformations in the Zermatt Valley (Figs. 5, 7) and thus opens new doors for satellite-based deformation detection in mountain environments. However, some limitations also exist as slant range direction does not always correspond to the dominating direction of ground deformation (Hu et al., 2014), as is the case for the slope direction of rock glaciers and slope normal direction for the accumulation of sediments on talus slopes (Kääb et al., 1997; Obanawa and Matsukura, 2008). Therefore, analysis along slant range direction may not necessarily be the most appropriate tool for the quantitative comparison of activity for these processes. However, ground deformation is not limited to the dominant direction; it can also be observed along other directions (Kääb et al., 1997; Lambiel and Delaloye, 2004; Lugon et al., 2004; Obanawa and Matsukura, 2008). This means that any analysis along the slant range direction can still be useful for a qualitative detection of ground deformation. In fact, the ratio of InSAR image pairs showing potential ground deformation has a clear and positive relationship with activity of rock glaciers and talus slopes in our case and based on a comparison with field surveys (Table 5), therefore implying that InSAR analyses are applicable to the estimation of activity in these geomorphic units.

As such, activity of rock glaciers and talus slopes is not only affected by sediment supply from rock cliffs, but also by the thermal and hydrological conditions of their permafrost bodies (Lambiel and Delaloye, 2004; Haeberli et al., 2006; Ikeda et al., 2008). Therefore, their activity does not solely reflect retreat rates of the rock cliffs located above them. Despite such a complexity, the positive relationship between the ratio of InSAR images showing deformation of rock cliffs and in-situ activity of rock glaciers and talus slopes just below the rock cliffs (Table 5) implies that InSAR analyses are a useful tool for a primary assessment of rock cliff activity and retreat.

Coherence of image pairs, which affects reliability of the InSAR analyses (Wegmuller and Werner, 1995; Jebur et al., 2014; Singleton et al., 2014), is low at rock cliffs steeper than 40° (Fig. 8A). In such areas, slopes facing northwest are sometimes affected by foreshortening and layover (as can be seen, e.g., on the left side of Fig. 5A), whereas slopes facing southeast are affected by radar shadow (e.g., around RC2 in Fig. 7B). Thus, ground-based InSAR will be better than space-borne InSAR when focusing on the deformation of rock cliffs. Low coherence of rock cliffs in high elevation areas (>3000 m asl) are also possibly affected by snow cover, which causes decorrelation in alpine environments (Kumar and Venkataraman, 2011). Coherence of other geomorphic units, including rock glaciers, talus slopes, moraines (in LIA and LG), landslide scars, and debris flow cones, mostly exceed 0.2 because of the gentler terrain (generally <40°) (Fig. 8A). Coherence of glaciers is clearly lower than at its surroundings (Fig. 5) because of the change in the geometrical configuration of the scatter (Frey et al., 2012). Low coherence areas outside the lower end of glaciers (e.g., north of G1 and G2 in Fig. 5) are likely related to the presence of debris-covered glaciers, in which decorrelation occurs because of the active motion of ice flow and surface-geometry changes by ice melt (Frey et al., 2012). Therefore, reliability of InSAR analyses differs between types of geomorphic units and is affected by their steepness, surface conditions, and altitude.

In the Alps, images for InSAR analysis are available only for the snow-free summer months. Therefore, analyses of image pairs in summers with an observation period of one year is effective when we assess activity of geomorphic processes including snow-cover seasons. This point is an advantage of analysis using L-band images because InSAR analyses with shorter wave length (i.e. C-band and X-band) cannot be completed for such long observation periods (Wei and Sandwell, 2010; Short et al., 2011). The L-band InSAR also has the advantage that slow geomorphic processes, which do not significantly change topography during short observation periods, can be detected by analysis of image pairs with a longer observation period.

5.2. Activity at geomorphic units

5.2.1 Rock glaciers

At our study site, many rock glaciers are on north-facing slopes, as in many other areas of Eastern Europe or North America (Johnson et al., 2007; Vespremeanu-Stroe et al., 2010). On south-facing slopes, direct solar radiation prevents the formation of permafrost, resulting in a predominance of talus slopes (Fig. 4).

Some 90% of the rock glaciers are in potential permafrost areas according to maps from Gruber and Hoelzle (2001) and based on elevation and potential solar radiation. Activity of rock glaciers peaks at elevations ranging between 2500 and 2750 m asl, corresponding to the lower boundary of permafrost occurrence in the areas (Gruber and Hoelzle, 2001). Previous studies reported that rock glaciers with temperatures close to the thawing point of permafrost tend to move much faster than colder rock glaciers (Ikeda et al., 2008; Lambiel and Delaloye, 2004; Stoffel and Huggel, 2012; Stoffel et al., 2014), which is in line with the findings of our InSAR analyses. Rock glaciers below this elevation (≈2750 m asl) are considered to be inactive or relict because of the degradation or absence of permafrost. The elevation of steep rock cliffs (>2750 m asl in the study area) also constrains the occurrence of rock glaciers because sediment supply affects the activity of rock glaciers (Burger et al., 1999; Humlum, 2000; Johnson et al., 2007).

Rock glacier activity changes with seasonal or interannual variability of internal temperatures (Hoelzle et al., 1998; Lambiel and Delaloye, 2004; Ikeda et al., 2008; Scapozza et al., 2014). Peak velocity of rock glaciers sometimes lags behind the warmest season by several months to half years, depending on the depth of the shear zone (Arenson et al., 2002). Thus, there is a possibility that we missed the most active season in periods 2 and 3 because data were taken during or just after the warmest time of the year (July and August). By contrast, period 1, for which the duration between two images was about 1 year, certainly includes the period(s) with peak velocity. In fact, the number of rock glaciers with potential deformation areas in period 1 exceeded that in the other two periods (21, 11, and 13 rock glaciers in periods 1, 2, and 3 respectively). At the same time, performing analysis of pairs with long observation periods bears the risk of decorrelation by heavy rain, strong wind, and changes to the ground surface caused by fallen leaves (Rosen et al., 1996; Chen et al., 2000; Ahmed et al., 2011). However, average coherence throughout the study area in period 1 (0.33), which has the longest observation period of 368 days, was not clearly lower than average coherence in the other 2 periods (0.37 in both), although they both had much shorter observation periods with 46 days.

5.2.2 Talus slopes

For talus slopes, the average ratio of images showing potential deformation at higher elevations (i.e., >2750 m asl) exceeds that observed at lower elevations (i.e., <2750 m asl; Fig. 3). In addition, the north-facing slopes show a larger ratio of images indicating deformation than those on south-facing slopes (Fig. 4), which is consistent with the higher possibility of the presence of permafrost (Lambiel and Pieracci, 2008; Scapozza et al., 2011). This indicates that deformation detected by the InSAR analyses is attributed to the creep of frozen sediments, together with the accumulation of new rockfall debris derived from rock cliffs. Such active deformation of talus slopes in permafrost areas was also observed in other regions in the Alps (Phillips et al., 2009; Scapozza et al., 2011; Müller et al., 2014). InSAR analyses also detected some deformation on talus slopes at lower elevations, such as the talus slope below Randa rockslide (TS2 in Fig. 7A), which is not underlain by permafrost. This suggests that InSAR analyses can also detect development of talus slopes because of sediment supply from rock cliffs and landslide scars in nonpermafrost environment.

5.2.3 Rock cliffs

On-site monitoring of rock cliff dynamics in the Swiss Alps suggests that seasonal freezing-thawing is the primary trigger of rockfalls (Stoffel et al., 2005; Perret et al., 2006) as it contributes to meter-scale deterioration of rock particularly under the presence of permafrost (e.g., Wegmann and Gudmundsson, 1999; Krautblatter and Hauck, 2007; Matsuoka, 2008; Girard et al., 2013). The freeze-thaw depth in the rock cliff, which controls the magnitude of rockfall, and consequently the retreat of rock cliff, is spatially variable with the slope direction and elevation (Gruber et al., 2004a, 2004b; Krautblatter and Hauck, 2007; Curtaz et al., 2014). In the study area, the ratio of images showing deformation was high on north-facing slopes, in particular at lower elevations (<3000 m asl), whereas the ratio was high on south-facing slopes but only for higher elevations (>3250 m; Table 6). This suggests that the elevation of slopes with active rock cliff retreat is variable with the slope direction.

5.2.4 Moraines

InSAR images indicate potential ground deformation in LIA moraines at elevations from 2500 to 3000 m asl (Fig. 3F). The ratio of images indicating deformation is higher on north-facing than on south-facing slopes. These characteristics agree with those for rock glaciers and talus slopes, indicating that permafrost creep also contributes to the deformation of ice-cored or ice-filled moraines, as supported by geophysical and geodetic observations of LIA moraines (Lugon et al., 2004; Kääb and Kneisel, 2006). By contrast, deformation of LG moraines, which are considered to be ice-free, cannot be found by InSAR analyses.

5.3. Geomorphic system in the Zermatt Valley

InSAR analyses in the entire study area show that the displacement of geomorphic units composed of rock debris (i.e., rock glaciers, talus slopes, LIA moraines) and the retreat of rock cliffs are currently most active at elevations above 2500 m asl, particularly on north-facing slopes (Fig. 3) where permafrost is widespread (Gruber and Hoelzle, 2001). These results agree with previous studies emphasizing the importance of permafrost on the development of Alpine landscapes (e.g., Lambiel and Delaloye, 2004; Harris et al., 2009; Kenner et al., 2014). Rock glaciers, talus slopes, and LIA moraines predominate at elevations between 2500 and 3000 m asl, where many glaciers terminate today (Fig. 3). There is a possibility that retreat of glacier, which is evident in the Swiss Alps (Paul and Haeberli, 2008; Pelliciotti et al., 2014), has generated unstable terrains and the exposure of unstable glacigenic material, facilitating deformation of geomorphic units (Johnson, 1984; Ballantyne, 2002; Delaloye et al., 2007, 2012; Stoffel and Huggel, 2012; Fey et al., 2017).

At lower elevations (<2250 m asl), the retreat of rock cliffs and landslide scars as well as the displacement of talus slopes (Fig. 3) indicates that sediment supply and transport, not related to permafrost, are also active. Although the occurrence of new landslides was not identified in the observation period, the occurrence of landslides, such as the Randa rockslide in 1991 (30 million m^3) (Willenberg et al., 2008a, 2008b), also supplies a large volume of sediment to the system.

In the northern part of the study area (around the validation area), almost no ground deformation was detected in the flat and gentle valley bottom of tributaries located at elevations 2400-2600 m asl formed by glaciers during the LG. No field evidence of recent floods was found in these valley bottoms. Debris flow cones are also limited (Fig. 2), indicating that sediment transport in these tributaries was not active during the study period; this was also confirmed by in situ observations (Schneuwly-Bollschweiler and Stoffel, 2012). Therefore, sediment with larger grain sizes supplied from rock cliffs is unlikely to reach the Mattervispa River via these gentle channel sections. In such areas, rock glaciers are considered to be an important sediment sink in the catchment (Müller et al., 2014). In the southern part of the study area (south of the Randa rockslide), glaciers that restrict fluvial sediment transport widely cover the valley bottom of the subcatchments (Fig. 2). Limited formation of debris flow cones in this area also indicates inactive sediment transport (e.g., debris flow) recently in these tributaries. By contrast, in the central part of the study area, many moraines, talus slopes, and rock glaciers, activities of which were identified by InSAR analyses, exist at the headwaters of the tributaries at 2500-2800 m a.s.l. (Figs. 2, 3). These tributaries lack gentle channel sections formed by the LG glaciers. Therefore, sediment supplied from rock cliffs can reach the Mattervispa River via moraines, talus slopes, and rock glaciers, and ultimately the tributaries. Although our DInSAR analysis could not detect any debris flows in the short observation period from 18 July 2008 to 21 October 2008, such a linkage between sediment supply and transport results in frequent debris flows (Lugon and Stoffel, 2010; Stoffel, 2010; Stoffel et al., 2014; Imaizumi et al., 2016, 2017). Formation of many debris flow cones in this area indicates frequent occurrence of debris flows (Fig. 2).

6. Conclusions

In this study, we interpreted activity of alpine geomorphic processes by geomorphic mapping and L-band DInSAR analyses in the Zermatt Valley, Swiss Alps. The ratio of image pairs detecting potential ground deformations in rock glaciers and talus slopes shows a positive relationship with their activity as interpreted by field surveys. Thus, L-band DInSAR analyses can be used to understand the activity of geomorphic processes in Alpine environments. The ratio of image pairs detecting potential deformation is high in the case of rock glaciers, talus slopes, and moraines near the lower limit of permafrost distribution on north-facing slopes. Thus, permafrost is an important factor controlling development of landscapes in this part of the Swiss Alps. The ratio of image pairs detecting potential deformation on rock cliffs has a positive relationship with in situ activity of rock glaciers and talus slopes below rock cliffs, implying that L-band DInSAR is also useful for the estimation of rock cliff activity and retreat. Our analyses therefore provide valuable insights into spatial differences in the sediment transport system from rock cliffs to the main river (Mattervispa River in this study), affected by catchment topography and the dominating gravitational processes.

In this study, we qualitatively interpreted the activity of various geomorphic processes over a large area by using a single method composed of geomorphic mapping and L-band DInSAR analyses. Because L-band DInSAR can analyze image pairs with observation periods longer than one year, geomorphic activity can be interpreted throughout all seasons. This method is effective as a primary interpretation to understand geomorphic processes, prior to a more detailed assessment such as laser scanning, GNSS monitoring, and/or any other type of field survey. As demonstrated in this study, the activity of alpine geomorphic processes is largely controlled by permafrost and glaciers, which are susceptible to being affected by climate change. Therefore, L-band SAR analyses and geomorphic mapping, which do not require a large budget and work, should also be an appropriate monitoring method to prevent geohazards over wide alpine areas.

Acknowledgement

This study was supported by JSPS Grant Numbers 17H02029. We are grateful to three anonymous reviewers for their constructive comments. Editor Richard A. Marston is thanked for his efforts on handling the manuscript.

References

Ahmed, R., Siqueira, P., Hensley, S., Chapman, B., Bergen, K., 2011. A survey of temporal decorrelation from spaceborne L-Band repeat-pass InSAR. Remote Sens. Environ. 115, 2887–2896. DOI:10.1016/j.rse.2010.03.017

Arenson, L., Hoelzle, M., and Springman, S., 2002. Borehole deformation measurements and internal structure of some rock glaciers in Switzerland, Permafrost and Periglac. Process. 13, 117–135. DOI: 10.1002/ppp.414.

Arosio, D., Longoni, L., Papini, M., Scaioni, M., Zanzi, L., and Alba, M., 2009. Towards rockfall forecasting through observing deformations and listening to microseismic emissions. Nat. Hazards Earth Syst. Sci. 9, 1119–1131. DOI: 10.5194/nhess-9-1119-2009.

Ballantyne, C.K., 2002. Paraglacial geomorphology. Quaternary Sci. Rev. 21, 1935–2017. DOI: 10.1016/S0277-3791(02)00005-7.

Bamler, R., Hartl, P., 1998. Synthetic aperture radar interferometry - TOPICAL REVIEW -. Inverse Problems 14, R1–R54. DOI: 10.1088/0266-5611/14/4/001

Barboux, C., Delaloye R., Lambiel, C., 2014. Inventorying slope movements in an Alpine environment using DInSAR, Earth Surf. Process. Landf. 39, 2087–2099. DOI: 10.1002/esp.3603.

Berger, J., Krainer, K., and Mostler, W., 2004. Dynamics of an active rock glacier (Ötztal Alps, Austria), Quat. Res. 233–242.

Bollschweiler, M., Stoffel, M., 2010. Variations in debris-flow occurrence in an Alpine catchment – A reconstruction based on tree rings. Glob. and Planet. Change 73, 186–192.

Burga, C.A., Frauenfelder, R. Ruffet, J. Hoelzle, M. Kääb, A., 2004. Vegetation on Alpine rock glacier surfaces: a contribution to abundance and dynamics on extreme plant habitats, Flora 199, 505–515.

Burger K.C., Degenhardt Jr. J.J., Giardino J.R., 1999. Engineering geomorphology of rock glaciers, Geomorphology 31, 93–132.

Chen, C., Zebker, H., 2002. Phase unwrapping for large SAR interferograms: statistical segmentation and generalized network models. IEEE Trans. Geosci. Remote Sens. 40, 1709–1719. DOI: 10.1109/tgrs.2002.802453.

Chen, Y., Zhang, G., Ding, X., Li, Z., 2000. Monitoring earth surface deformations with InSAR technology: principles and some critical issues. J. Geosp. Eng. 2 (1), 3–22.

Curtaz M.A., Ferrero, M., Roncella, R., Segalini, A., Umili G., 2014. Terrestrial Photogrammetry and Numerical Modelling for the Stability Analysis of Rock Slopes in High Mountain Areas: Aiguilles Marbrées case, Rock Mechanics and Rock Engineering 47, 605–620. DOI: 10.1007/s00603-013-0446-z.

Delaloye, R., Lambiel, C., Lugon, R., Raetzo, H., Strozzi, T., 2007. Typical ERS InSAR signature of slope of slope movements in a periglacial mountain environment, Swiss Alps. In proceedings of *ENVISAT Symposium 2007*, (ESA SP-636, July 2007).

Delaloye, R., Lambiel, C., Gärtner-Roer, I., 2010. Overview of rock glacier kinematics research in the Swiss Alps, Geog. Helvetica 65, 135–145.

Delaloye, R., Morard, S., Barboux, C., Abbet, D., Gruber, V., Riedo, M., Gachet S., 2012. Rapidly moving rock glaciers in Mattertal, Jahrestagung der Schweizerischen Geomorphologischen Gesellschaft, 21–31.

Fey, C., Wichmann, V., Zangerl, C. 2017. Reconstructing the evolution of a deep seated rockslide (Marzell) and its response to glacial retreat based on historic and remote sensing data. Geomorphology 298, 72–85.

Fischer, L, Purves, R.S., Huggel, C., Noetzli, J., Haeberli, W., 2012. On the influence of topographic, geological and cryospheric factors on rock avalanches and rockfalls in high-mountain areas, Nat. Hazards Earth Syst. Sci. 12, 241–254. DOI: 10.5194/nhess-12-241-2012.

Frey, H., Paul, F., Strozzi, T., 2012. Compilation of a glacier inventory for the western Himalayas from satellite data: methods, challenges, and results. Remote Sens. of Environ. 124, 832–843. DOI: 10.1016/j.rse.2012.06.020.

García-Davalillo, J.C., Herrera, G., Notti, D., Strozzi, T., Álvarez-Fernández, I., 2014. DInSAR analysis of ALOS PALSAR images for the assessment of very slow landslides: the Tena Valley case study, Landslides 11, 225–246, DOI 10.1007/s10346-012-0379-8

Girard, L., Gruber, S., Weber, S. Beutel, J., 2013. Environmental controls of frost cracking revealed through in situ acoustic emission measurements in steep bedrock. Geophys. Res. Lett. 40, 1748–1753.

Graham, R.L., Hell, P., 1985. On the History of the Minimum Spanning Tree Problem. Ann. Hist. Comput. 7, 43–57. DOI: 10.1109/mahc.1985.10011.

Gruber S., Hoelzle, M., 2001. Statistical Modelling of Mountain Permafrost Distribution: Local Calibration and Incorporation of Remotely Sensed Data, Permafrost and Periglac. Process. 12, 69–77. DOI: 10.1002/ppp 374.

Gruber S., Hoelzle, M. Haeberli W., 2004a. Permafrost thaw and destabilization of Alpine rock walls in the hot summer of 2003, Geophys. Res. Lett. 31, L13504. DOI:10.1029/2004GL020051.

Gruber, S., Hoelzle, M., Haeberli W., 2004b. Rock-wall temperatures in the Alps: Modelling their topographic distribution and regional differences, Permafrost and Periglac. Process. 15, 299–307. DOI: 10.1002/ppp.501.

Haeberli W., Hallet B., Arenson L., Elconin R., Humlum O., Kääb A., Kaufmann V., Ladanyi B., Matsuoka N., Springman S., Mühll D.V., 2006. Permafrost creep and rock glacier dynamics. Permafrost Periglac. Process. 17, 189–214.

Hamilton, S.J., Whalley, W.B., 1995. Preliminary results from the lichenometric study of the Nautardalur rock glacier, Trollaskagi, northern Iceland, Geomorphology 12, 123–132.

Harris, C., Arenson, L.U., Christiansen, H.H., Etzelmüller, B., Frauenfelder, R., Gruber, S., Haeberli, W., Hauck, C., Hölzle, M., Humlum, O., Isaksen, K., Kääb, A., Kern-Lütschg, M., Lehning, M., Matsuoka, N., Murton, J.B., Nötzli, J., Phillips, M., Ross, N., Seppälä, M., Springman, S.M., Vonder Mühll, D., 2009. Permafrost and climate in Europe: monitoring and modelling thermal, geomorphological and geotechnical responses. Earth Sci. Rev. 92, 117–171.

Hoelzle, M., Wagner, S., Kääb, A., Vonder Mühll, D., 1998. Surface movements and internal deformation of ice-rock mixtures within rock glaciers at Pontresina-Schafberg, Upper Engadin, Switzerland. In Proceedings of the 7th International Conference on Permafrost, Yellowknife. Nordicana 57, Universit´e Laud, 465–471.

Hu, J., Li, Z.W., Ding, X.L., Zhu, J.J., Zhang, L., Sun, Q., 2014. Resolving three-dimensional surface displacements from InSAR measurements: A review, Earth-Sci. Rev. 133, 1–17. DOI: 10.1016/j.earscirev.2014.02.005.

Humlum, O., 2000. The geomorphic significance of rock glaciers: estimates of rock glacier debris volumes and headwall recession rates in W Greenland. Geomorphology 35, 41–67.

Ikeda, A., Matsuoka, N., 2002. Degradation of Talus-derived Rock Glaciers in the Upper Engadin, Swiss Alps. Permafrost and Periglac. Process. 13, 145–161. DOI: 10.1002/ppp.413.

Ikeda, A., Matsuoka, N., Kääb, A., 2008. Fast deformation of perennially frozen debris in a warm rock glacier in the Swiss Alps: An effect of liquid water. J. Geophys. Res. 113, F01021, DOI:10.1029/2007JF000859.

Imaizumi, F., Trappman, D., Matsuoka, N., Tsuchiya, S., Ohsaka, O., Stoffel, M., 2016. Biographical sketch of a giant: deciphering recent debris-flow dynamics from Ohya landslide body (Japanese Alps). Geomorphology 272, 102–114.

Imaizumi, F., Hayakawa, Y.S., Hotta, N., Tsunetaka, H., Ohsaka, O., Tsuchiya, S., 2017. Relationship between the accumulation of sediment storage and debris flow characteristics in a debris-flow initiation zone, Ohya landslide body, Japan. Nat. Hazards Earth Syst. Sci. 17, 1923–1938. https://doi.org/10.5194/nhess-17-1923-2017.

Jebur, M.N., Pradhan, B., Tehrany, M.S., 2014. Detection of vertical slope movement in highly vegetated tropical area of Gunung pass landslide, Malaysia, using L-band InSAR technique. Geosci. J. 18, 61–68. DOI: 10.1007/s12303-013-0053-8.

Joerin, U.E., Stocker, T.F., Schlüchter, C., 2006, Multicentury glacier fluctuations in the Swiss Alps during the Holocene. The Holocene 16, 697–704.

Johnson, B.G., Thackray, G.D., Van Kirk, R., 2007. The effect of topography, latitude, and lithology on rock glacier distribution in the Lemhi Range, central Idaho, USA. Geomorphology 91, 38–50.

Johnson, P.G., 1984. Rock glacier formation by high-magnitude low-frequency slope processes in the southwest Yukon. Annals of the Association of American Geographers 74, 408–419.

Kääb, A, Kneisel C., 2006. Permafrost Creep within a Recently Deglaciated Glacier Forefield: Muragl, Swiss Alps. Permafrost and Periglac. Process. 17, 79–85. DOI: 10.1002/ppp.540.

Kääb, A., Haeberli, W., Gudmundsson, G.H., 1997. Analysing the Creep of Mountain Permafrost using High Precision Aerial Photogrammetry: 25 Years of Monitoring Gruben Rock Glacier, Swiss Alps. Permafrost and Periglac. Process. 8, 409–426.

Kenner, R., Bühler, Y., Delaloye, R., Ginzler, C., Phillips, M., 2014. Monitoring of high alpine mass movements combining laser scanning with digital airborne photogrammetry. Geomorphology 206, 492–504.

Korup, O., Densmore, A.L., Schlunegger, F., 2010. The role of landslides in mountain range evolution. Geomorphology 120, 77–90. https://doi.org/10.1016/j.geomorph.2009.09.017

Krautblatter, M., Hauck, C., 2007. Electrical resistivity tomography monitoring of permafrost in solid rock walls. J. Geophys. Res. 112, F02S20, DOI: 10.1029/2006JF000546.

Kumar, V., Venkataraman, G., 2011. Interferometric coherence analysis for snow cover mapping in the western Himalayan region. J. Digital Earth 4, 78–90.

Lambiel C., Delaloye, R., 2004. Contribution of real-time kinematic GPS in the study of creeping mountain permafrost: examples from the Western Swiss Alps. Permafrost and Periglac. Process. 15, 229–241. DOI: 10.1002/ppp.496.

Lambiel C., Pieracci, K., 2008. Permafrost distribution in talus slopes located within the Alpine Periglacial Belt, Swiss Alps. Permafrost and Periglac. Process. 19, 293–304. DOI: 10.1002/ppp.624.

Liu, L., Zhang, T., Wahr, J., 2010. InSAR measurements of surface deformation over permafrost on the North Slope of Alaska. J. Geophys. Res. 115, F03023. DOI: 10.1029/2009JF001547.

Liu, L., Millar, C.I., Westfall, R.D., Zebker, H.A., 2013. Surface motion of active rock glaciers in the Sierra Nevada, California, USA: inventory and a case study using InSAR. The Cryosphere 7, 1109–1119.

Lu, Z., Dzurisin, D., Biggs Wicks, J.C. Jr, McNutt, S., 2010. Ground surface deformation patterns, magma supply, and magma storage at Okmok volcano, Alaska, from InSAR analysis: 1. Intereruption deformation, 1997–2008. J. Geophys. Res. 115, B00B02. DOI: 10.1029/2009JB006969.

Lugon., R., Stoffel, M., 2010. Rock-glacier dynamics and magnitude–frequency relations of debris flows in a high-elevation watershed: Ritigraben, Swiss Alps. Global and Planetary Change 73, 202–210. DOI:10.1016/j.gloplacha.2010.06.004.

Lugon, R., Delaloye, R., Serrano, E., Reynard, E., Lambiel, C., Gonza´lez-Trueba, J.J., 2004. Permafrost and little ice age glacier relationships, Posets Massif, Central Pyrenees, Spain. Permafrost and Periglac. Process. 15, 207–220, DOI: 10.1002/ppp.494.

Matsuoka, N., 2008. Frost weathering and rockwall erosion in the eastern Swiss Alps: Long-term (1994-2006) observations. Geomorphology 99, 353–368.

Müller, J., Gärtner-Roer, I., Kenner, R., Thee, P., Morche, D., 2014. Sediment storage and transfer on a periglacial mountain slope (Corvatsch, Switzerland), Geomorphology 218, 35–44. https://doi.org/10.1016/j.geomorph.2013.12.002

Nishiguchi, T., Tsuchiya, S., Imaizumi, F., 2017. Detection and accuracy of landslide movement by InSAR analysis using PALSAR-2 data. Landslides 14, 1483–1490. DOI: 10.1007/s10346‑017‑0821‑z.

Obanawa, H., Matsukura, Y., 2008. Cliff retreat and talus development at the caldera wall of Mount St. Helens: Computer simulation using a mathematical model. Geomorphology 97, 697–711.

Oliveira, S.C. , Zêzere, J.L., Catalão, J., Nico G., 2015. The contribution of PSInSAR interferometry to landslide hazard in weak rock-dominated areas. Landslides 12, 703–719. DOI: 10.1007/s10346-014-0522-9.

Otto, J., Schrott, J., Jaboyedoff, M., Dikau, R., 2009. Quantifying sediment storage in a high alpine valley (Turtmanntal, Switzerland), Earth Surf. Process. Landf. 34, 1726–1742. DOI: 10.1002/esp.1856.

Ozawa, T., Fujita, E., Ueda, H., 2016. Crustal deformation associated with the 2016 Kumamoto Earthquake and its effect on the magma system of Aso volcano. Earth. Pl. Sp. 68 (1). DOI: 10.1186/s40623-016-0563-5.

Paul, F., Haeberli, W., 2008. Spatial variability of glacier elevation changes in the Swiss Alps obtained from two digital elevation models. Geophys. Res. Lett. 35, L21502. DOI: 10.1029/2008GL034718.

Pellicciotti F., Carenzo M., Bordoy, R., Stoffel, M., 2014. Changes in glaciers in the Swiss Alps and impact on basin hydrology: Current state of the art and future research. Science of the Total Environment 493, 1152–1170.

Perret, A., Stoffel, M., Kienholz, H., 2006. Spatial and temporal rockfall activity in a forest stand in the Swiss Prealps—A dendrogeomorphological case study, Geomorphology, 74 219–231.

https://doi.org/10.1016/j.geomorph.2005.08.009.

Peyret, M., Djamour, Y., Rizza, M., Ritz, J., Hurtrez, J., Goudarzi, M., Uri, F., 2008. Monitoring of the large slow Kahrod landslide in Alborz mountain range (Iran) by GPS and SAR interferometry. Eng. Geol. 100, 131–141. DOI: 10.1016/j.enggeo.2008.02.013

Phillips, M., Mutter, E.Z., Kern-Luetschg, M., Lehning, M., 2009. Rapid Degradation of Ground Ice in a Ventilated Talus Slope: Flüela Pass, Swiss Alps. Permafrost and Periglac. Process. 20, 1–14.

Roer, I., Haeberli, W. Avian, M., Kaufmann, V., Delaloye, R., Lambiel, C., Kääb, A., 2008. Observations and considerations on destabilizing active rock glaciers in the European Alps, Ninth International Conference on Permafrost 2, 1505–1510.

Roering, J.J., Stimley, L.L., Mackey, B.H., Schmidt, D.A., 2009. Using DInSAR, airborne LiDAR, and archival air photos to quantify landsliding and sediment transport. Geophys. Res. Lett. 36, L19402.

Rosen, P.A., Hensley, S., Zebker, H.A., Webb, F.H., Fielding, E.J., 1996. Surface deformation and coherence measurements of Kilauea Volcano, Hawaii, from SIR-C radar interferometry. J. Geophys. Res. 101 (E10), 23109–23125. DOI:10.1029/96je01459

Rouyet, L., Kristensen, L., Derron, M.H., Michoud, C., Blikra L.H., Jaboyedoff, M., Lauknes, T.M., 2017. Evidence of rock slope breathing using ground-based InSAR, Geomorphology 289, 152–169. https://doi.org/10.1016/j.geomorph.2016.07.005

Saroli, M., Stramondo S, Moro M, Doumaz F., 2005. Movements detection of deep seated gravitational slope deformations by means of InSAR data and photogeological interpretation: northern Sicily case study, Terra Nova 17, 35–43. https://doi.org/10.1111/j.1365-3121.2004.00581.x.

Scapozza, C, Lambiel, C, Baron, L., Marescot, L., Reynard, E., 2011. Internal structure and permafrost distribution in two alpine periglacial talus slopes, Valais, Swiss Alps, Geomorphology 132, 208–221. https://doi.org/10.1016/j.geomorph.2011.05.010.

Scapozza, C., Lambiel, C., Bozzini, C., Mari, S., Conedera, M., 2014. Assessing the rock glacier kinematics on three different timescales: a case study from the southern Swiss Alps, Earth Surf. Process. Landf. 39, 2056–2069, DOI: 10.1002/esp.3599.

Schaefer, L.N., Lu, Z., Oommen, T., 2015. Dramatic volcanic instability revealed by InSAR, Geology 43, 743–746. DOI: 10.1130/G36678.1

Schneuwly-Bollschweiler, M., Stoffel, M., 2012. Hydrometeorological triggers of periglacial debris flows in the Zermatt Valley (Switzerland) since 1864. J. Geophys. Res. 117, F02033.

Short, N., Brisco, B., Couture, N., Pollard, W., Murnaghan, K., Budkewitsch, P., 2011. A comparison of TerraSAR-X, RADARSAT-2 and ALOS-PALSAR interferometry for monitoring permafrost environments, case study from Herschel Island, Canada. Remote Sens. Environ. 115, 3491-3506. DOI:10.1016/j.rse.2011.08.012.

Singleton, A., Li, Z., Hoey, T., Muller, J.P., 2014. Evaluating sub-pixel offset techniques as an alternative to D-InSAR for monitoring episodic landslide movements in vegetated terrain, Remote Sens. Environ. 147, 133–144. DOI: 10.1016/j.rse.2014.03.003

Stoffel, M., 2010. Magnitude-frequency relationships of debris flows – a case study based on field surveys and tree-ring records. Geomorphology 116, 67–76.

Stoffel, M., Huggel, C., 2012. Effects of climate change on mass movements in mountain environments. Progress in Physical Geography 36, 421–439.

Stoffel, M., Lièvre, I., Monbaron, M., Perret, S., 2005. Seasonal timing of rockfall activity on a forested slope at Täschgufer (Valais, Swiss Alps) – a dendrochronological approach. Z Geomorphol 49(1), 89–106.

Stoffel, M., Butler, D. R., Corona, C., 2013. Mass movements and tree rings: A guide to dendrogeomorphic field sampling and dating. Geomorphology 200, 106–120.

Stoffel, M, Tiranti D, Huggel, C., 2014. Climate change impacts on mass movements — Case studies from the European Alps. Sci. Total Environ. 493, 1255–1266.

Strozzi, T., Farina, P., Corsini, A., Ambrosi, C., Thüring, M., Zilger, J., Werner, C., 2005. Survey and monitoring of landslide displacements by means of L-band satellite SAR interferometry. Landslides 2, 193–201. DOI: 10.1007/s10346-005-0003-2

Strzelczyk, J., Porzycka, S., Lesniak, A., 2009. Analysis of ground deformations based on parallel geostatistical computations of PSInSAR data. 2009 17th International Conference on Geoinformatics 195–206. DOI: 10.1109/geoinformatics.2009.5293261.

Vespremeanu-Stroe, A., Urdea, P., Popescu, R., Vasile, M., 2010. Rock Glacier Activity in the Retezat Mountains, Southern Carpathians, Romania. Permafrost and Periglac. Process. 23, 127–137. DOI: 10.1002/ppp.1736.

Wegmann, M., Gudmundsson, G.H., 1999. Thermally induced temporal strain variations in rock walls observed at subzero temperatures. in *Advances in Cold-Region Thermal Engineering and Sciences* edited by Hutter, K., Wang, Y. and Beer, H., Springer, 511–518.

Wegmuller, U., Werner, C., 1995. SAR interferometric signatures of forest. IEEE Trans. Geosci. Remote. Sens. 33, 1153–1161. DOI: 10.1109/36.469479.

Wei, M., Sandwell, D. T., 2010. Decorrelation of L-Band and C-Band Interferometry Over Vegetated Areas in

California. IEEE Trans. Geosci. Remote. Sens. 48, 2942–2952. DOI: 10.1109/tgrs.2010.2043442.

Willenberg, H., Evans, K.F., Eberhardt, E., Spillmann, T., Loew, S., 2008a. Internal structure and deformation of an unstable crystalline rock mass above Randa (Switzerland): Part II — Three-dimensional deformation patterns, Eng. Geol. 101, 15–32.

Willenberg, H., Loewa, S., Eberhardt, E., Evans, K.F., Spillmann, T., Heincke, B., Maurer, H., Green, A.G., 2008b. Internal structure and deformation of an unstable crystalline rock mass above Randa (Switzerland): Part I — Internal structure from integrated geological and geophysical investigations, Engineering Geology 101, 1–14.

Wirz, V., Geertsema, M., Gruber, S., Purves, R. S., 2016. Temporal variability of diverse mountain permafrost slope movements derived from multi-year daily GPS data, Mattertal, Switzerland. Landslides 13, 67–83.

Zebker, H., Villasenor, J., 1992. Decorrelation in interferometric radar echoes. IEEE Trans. Geosci. Remote. Sens. 30, 950–959. DOI: 10.1109/36.175330.

Table 1

List of geomorphic units interpreted in this study

Unit name	Features of the geomorphic units	Number of identified units
Rock glacier	Gentler terrain in its upper part and steeper slope angles at the tongue.	31
Talus slope	Convex or linear cross-sectional topography with smooth surface. Diffuse tongue at the lower end of the deposits.	38
Rock cliff	Exposure of bedrock on steep slopes and lack of vegetation. Limited deposition of weathered material.	90
Landslide scar	Landslides that occurred before 2005 but for which a clear landslide topography persists over the time window analyzed (i.e., head scarp, conceived topography). Rockslides (e.g., Randa rockslide) and slope failures were included.	14
Moraine	Accumulation of unconsolidated debris in lateral and/or frontal parts of contemporary and past glaciers. Moraines are separated into those formed during the late glacial (LG), which are largely covered by vegetation, as well as those formed during glacier advances of the Little Ice Age (LIA), which are vegetation-free.	21 (LG 11, LIA 10)
Glacier	Gentler areas continuously covered with ice.	15
Debris flow cone	Cone-shaped topography along mountain rivers and torrents, usually formed at the outlet of steep terrains.	9

Table 2

PALSAR images analyzed in this study

Period	Observation date		Observation periods (days)	Baseline perpendicular (m)
	Master	Slave		
1	July 18, 2008	July 21, 2009	368	-355.2
2	July 21, 2009	September 5, 2009	46	606.0

3	September 5, 2009	October 21, 2009	46	395.1

Table 3

Classification of geomorphic process activity based on field surveys

Activity	Features of the geomorphic units
(a) Rock glaciers	
1 (inactive)	Recovery of vegetation or regolith, gentle topography at the base of the front
2 (active)	Recovery of lichens, relatively gentle topography at the lowermost part of the tongue
3 (very active)	Limited recovery of lichens, steep topography (> 40°) in the lowermost parts of the tongue, existence of wrinkles and cracks on its surface
(b) Talus slopes	
1 (inactive)	Recovery of vegetation or regolith over the entire slope
2 (active)	Recovery of vegetation or regolith with some new deposition (fresh clasts)
3 (very active)	Cover of fresh sediment over the entire slope without recovery of vegetation and regolith

Table 4

Average ratio of InSAR images showing ground deformation in the validation area

Geomorphic Units	Number of units classified by field surveys			Average ratio of images showing deformation		
	Activity 1 (inactive)	Activity 2 (active)	Activity 3 (very active)	Activity 1 (inactive)	Activity 2 (active)	Activity 3 (very active)
Rock glacier	5	6	6	0.20	0.50	0.67
Talus slope	3	5	4	0.11	0.13	0.42
Rock cliff	8	11	6	0.17	0.30	0.33

Table 5

Average ratio of InSAR images showing ground deformation, excluding low coherence geomorphic units

Geomorphic Units	Average coherence ≥ 0.15			Average coherence ≥ 0.20			Average coherence ≥ 0.25		
	Act. 1	Act. 2	Act. 3	Act. 1	Act. 2	Act. 3	Act. 1	Act. 2	Act. 3
Rock glacier	0.20	0.50	0.67	0.20	0.50	0.65	0.20	0.50	0.63
Talus slope	0.11	0.13	0.42	0.00	0.14	0.30	0.00	0.08	0.25
Rock cliff	0.17	0.30	0.33	0.09	0.28	0.29	0.10	0.22	0.27

Table 6

Ratio of images showing ground deformations in rock cliffs (numbers in brackets indicate the number of rock cliffs)[a]

Elevation (m asl)	Average ratio of images detecting deformation	
	North-facing slopes (W-N-E)	South-facing slopes (E-S-W)
<3000	0.37 (7)	0.27 (20)
3000-3250	0.27 (11)	0.29 (12)
>3250	0.21 (12)	0.56 (3)

[a] Average elevation and slope direction of the geomorphic units were used for the classification in the statistics.

Geomorphic units with average coherence <0.20 were excluded from analysis.

Figure captions

Fig. 1. Topographic map and view of typical geomorphic units in the study area. (A) Topographic map of the study area located on the east-facing slopes of the Zermatt Valley, west of the Mattervispa River. (B) Detailed view of one of the higher-elevation areas (2500–3500 m asl.), where glacial and periglacial landscapes are predominant. (C) View of one of the lower-elevation areas (1000–2000 m asl), where landslides and rockfalls prevail on the steep slopes.

Fig. 2. Geomorphic map of the study area. (A) Northern part of the study area including the validation area. (B) Southern part of the study area. Location of the two figures is shown in Fig. 1. LIA = Little Ice Age; LG = Late Glacial.

Fig. 3. Area ratio of geomorphic units for each elevational class with respect to the entire area of geomorphic units. Ratio of images showing potential ground deformations for each elevation class is shown as well. (A) Area ratio in the entire study area. (B) Rock glacier. (C) Talus slope. (D) Rock cliff. (E) Glacier. (F) Little Ice Age (LIA) and Late Glacial (LG) moraines. (G) Landslide scar. (H) Debris flow cone. Ratios of images showing ground deformations in the elevation classes with <3 units classified into the analyzing geomorphic type are not shown in the figure because representation of the analytical results is uncertain. Ratio of images showing deformation in glaciers is not shown because average coherence in all glaciers was below 0.2.

Fig. 4. Area ratio of geomorphic units in each direction to the entire area of the geomorphic units. Ratio of images showing ground deformations in each direction is also shown in the figure. Ratio of images showing ground deformations in the direction in which number of the units classified into the analyzing geomorphic type was <3 are not shown in the figures because representation of the analysis results is uncertain.

Fig. 5. Results of the InSAR analyses around the validation area. The upper maps illustrate displacement along the slant range direction obtained by InSAR analyses in period 1 (A), period 2 (B), and period 3 (C). The lower maps show coherence of the InSAR analyses for the corresponding areas in period 1 (D), period 2 (E), and period 3 (F).

Fig. 6. Number of InSAR images showing deformation in each geomorphic unit around the validation area. Activities of the rock glacier and the talus slopes interpreted by field surveys are also shown in the figure.

Fig. 7. Results of the InSAR analyses around the Randa rockslide (named as LS2 in the figure). Displacement along the slant range direction obtained by InSAR analyses in period 1 (A), period 2 (B), and period 3 (C). Coherence of the InSAR analyses in period 1 (D), period 2 (E), and period 3 (F) are also shown.

Fig. 8. Comparison between topographic factors and average coherence for each geomorphic unit with (A) slope gradient; (B) slope direction; and (C) elevation. Geomorphic units with erroneous values (e.g., layover, foreshortening, and radar shadow) are also plotted in the figure to explain the topographic conditions that gave the erroneous results.

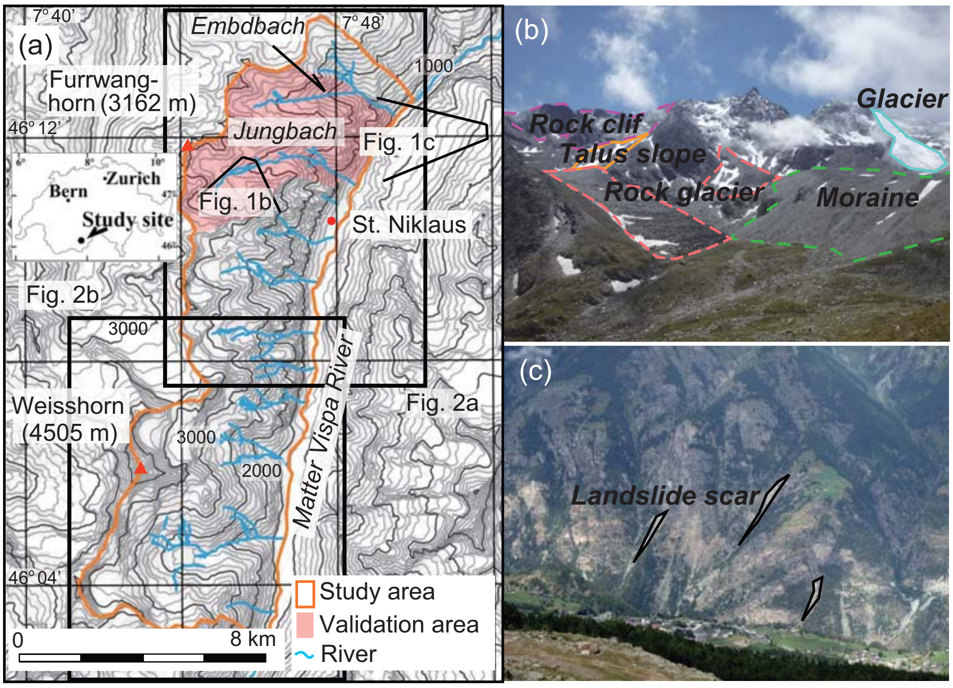
(a)
7° 40'
7° 48'
Embdbach
Furrwang-horn (3162 m)
1000
46° 12'
Jungbach
Fig. 1c
Fig. 1b
Zurich
Bern
Study site
St. Niklaus
Fig. 2b
3000
Weisshorn (4505 m)
Fig. 2a
3000
2000
Matter Vispa River
46° 04'
Study area
Validation area
River
0
8 km
(b)
Rock clif
Talus slope
Rock glacier
Moraine
Glacier
(c)
Landslide scar

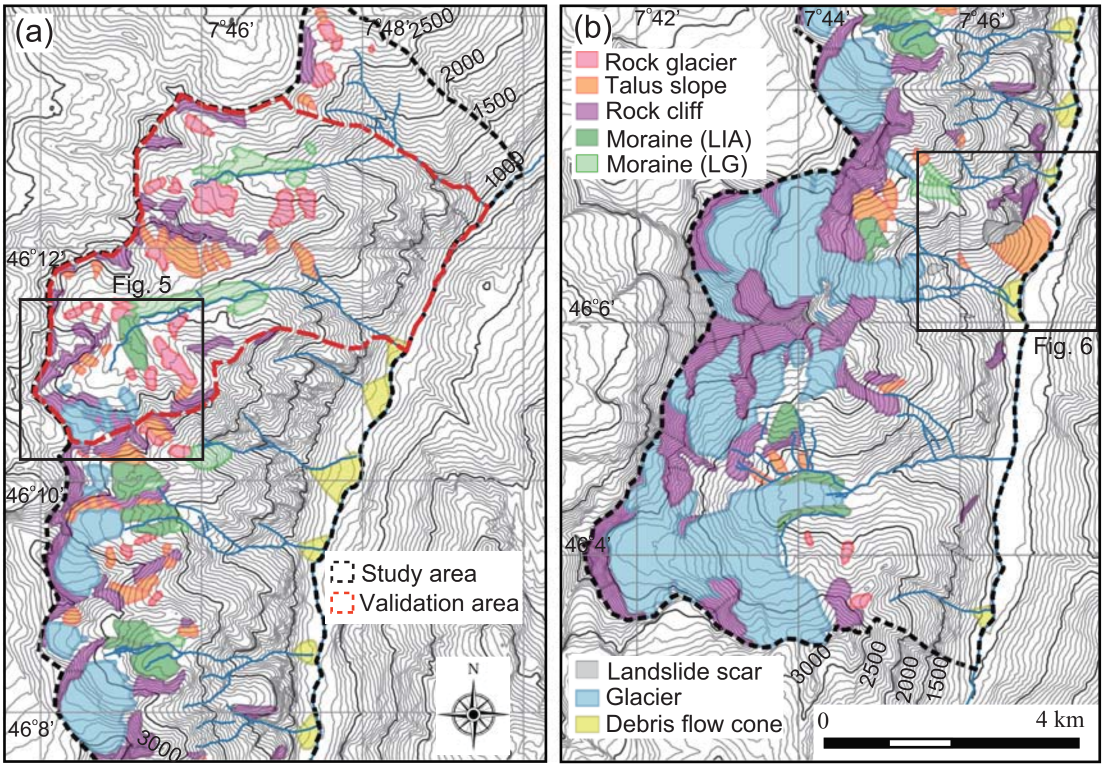
(a)
7°46'
7°48'
2500
2000
1500
1000
46°12'
Fig. 5
46°10'
46°8'
3000
Study area
Validation area
N
(b)
7°42'
7°44'
7°46'
Rock glacier
Talus slope
Rock cliff
Moraine (LIA)
Moraine (LG)
46°6'
Fig. 6
46°4'
Landslide scar
Glacier
Debris flow cone
3000
2500
2000
1500
0
4 km

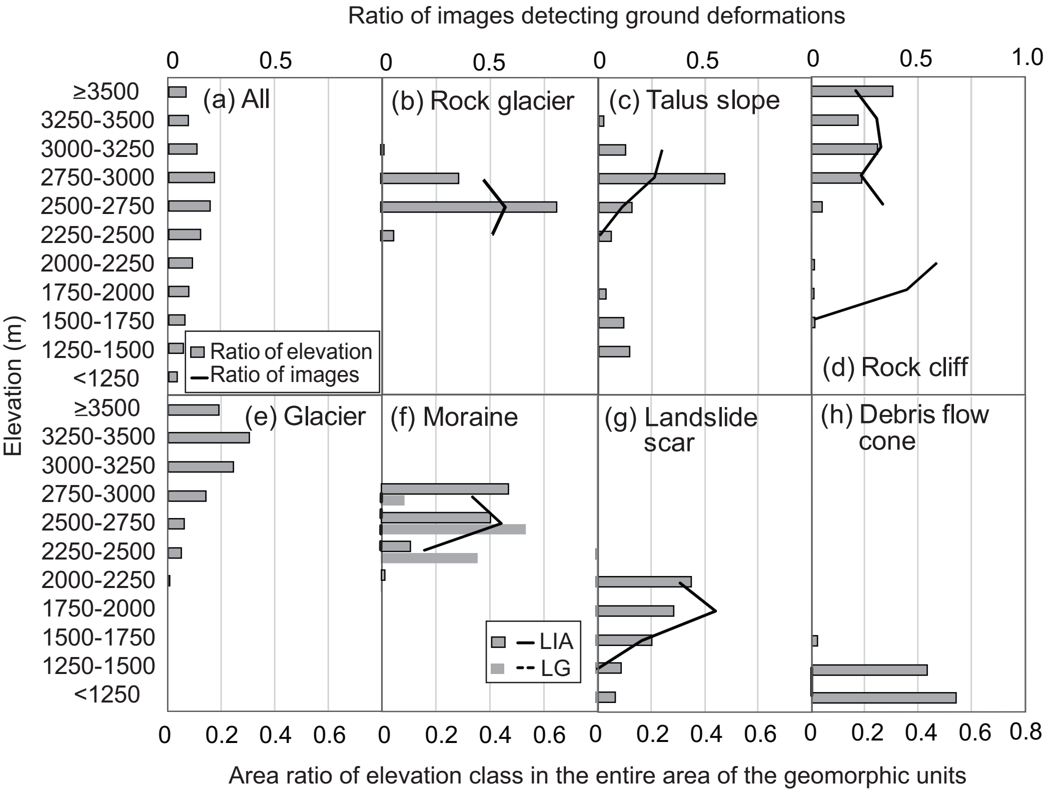
Ratio of images detecting ground deformations
0
0.5
0
0.5
0
0.5
0
0.5
1.0
(a) All
(b) Rock glacier
(c) Talus slope
(d) Rock cliff
(e) Glacier
(f) Moraine
(g) Landslide scar
(h) Debris flow cone
Ratio of elevation
Ratio of images
LIA
LG
Elevation (m)
≥3500
3250-3500
3000-3250
2750-3000
2500-2750
2250-2500
2000-2250
1750-2000
1500-1750
1250-1500
<1250
0
0.2
0.4
0.6
0
0.2
0.4
0.6
0
0.2
0.4
0.6
0
0.2
0.4
0.6
0.8
Area ratio of elevation class in the entire area of the geomorphic units

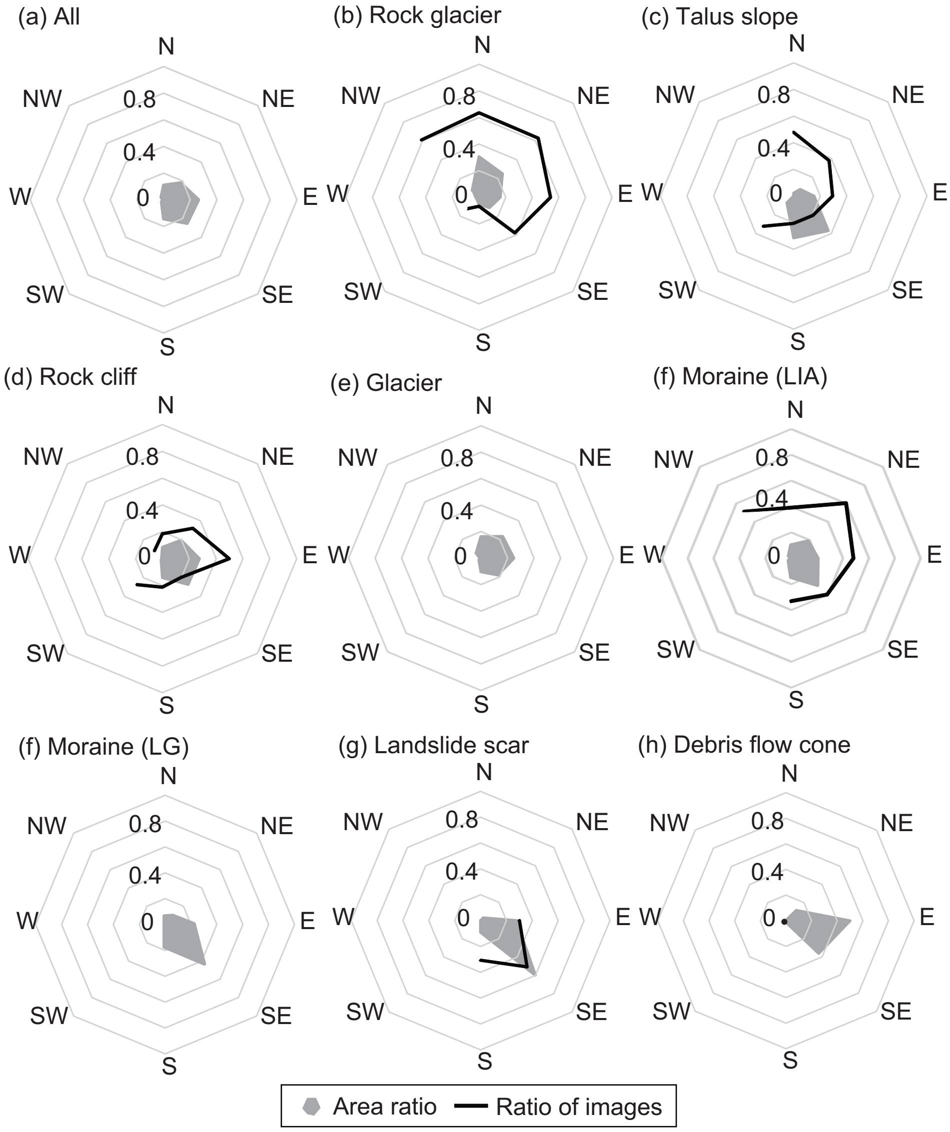
(a) All
(b) Rock glacier
(c) Talus slope
(d) Rock cliff
(e) Glacier
(f) Moraine (LIA)
(f) Moraine (LG)
(g) Landslide scar
(h) Debris flow cone
N
NE
E
SE
S
SW
W
NW
0
0.4
0.8
Area ratio
Ratio of images

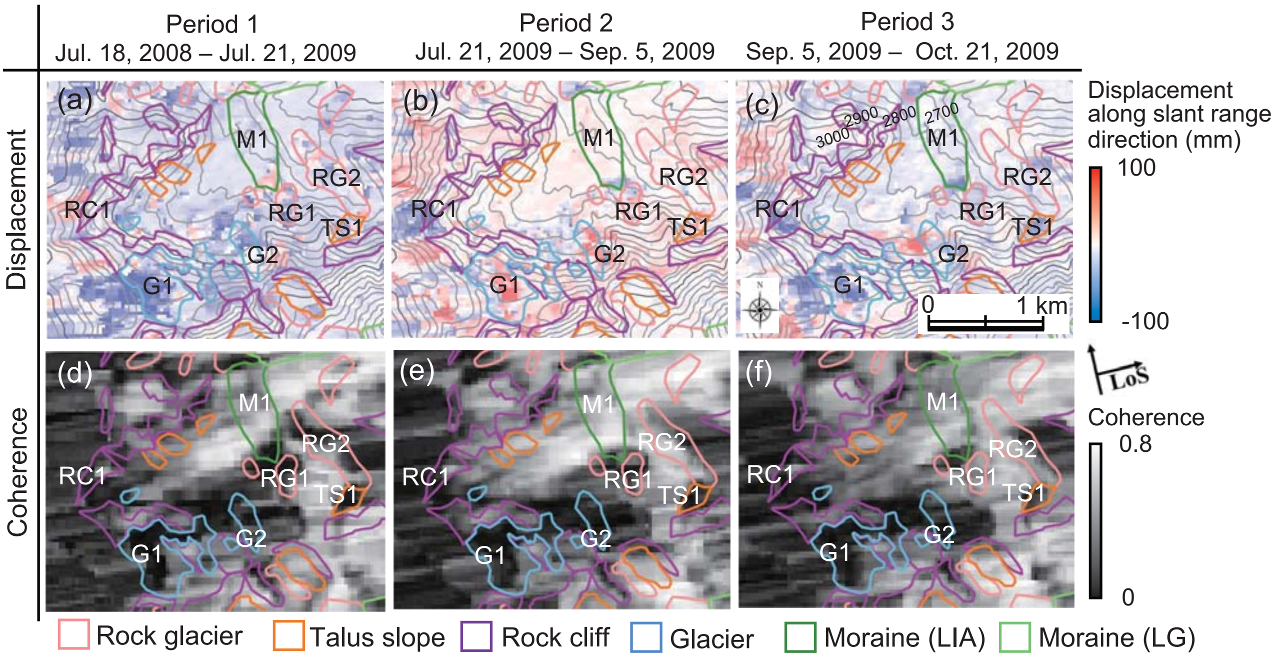
Period 1
Jul. 18, 2008 – Jul. 21, 2009
Period 2
Jul. 21, 2009 – Sep. 5, 2009
Period 3
Sep. 5, 2009 – Oct. 21, 2009
Displacement
Coherence
(a)
(b)
(c)
(d)
(e)
(f)
M1
RG2
RC1
RG1
TS1
G2
G1
3000
2900
2800
2700
0
1 km
Displacement along slant range direction (mm)
100
-100
LoS
Coherence
0.8
0
Rock glacier
Talus slope
Rock cliff
Glacier
Moraine (LIA)
Moraine (LG)

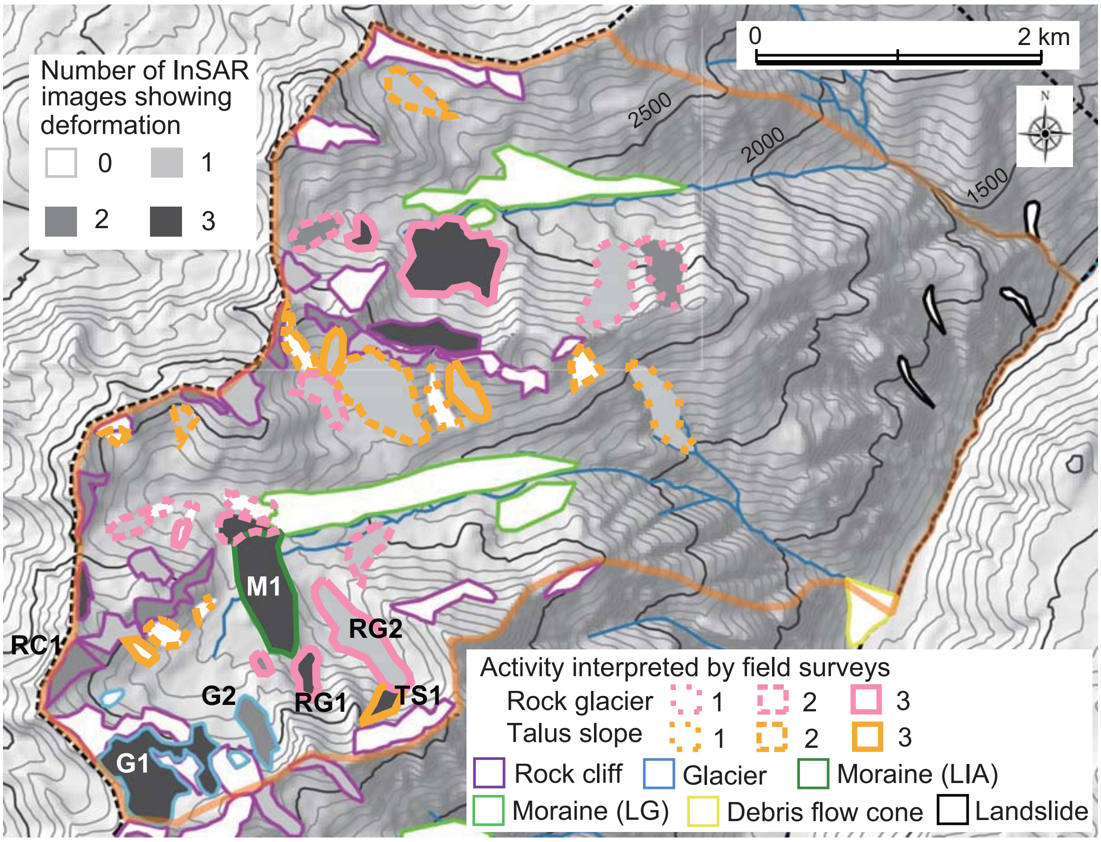
Number of InSAR images showing deformation
0
1
2
3
0
2 km
N
2500
2000
1500
M1
RG2
RC1
G2
RG1
TS1
G1
Activity interpreted by field surveys
Rock glacier 1 2 3
Talus slope 1 2 3
Rock cliff
Glacier
Moraine (LIA)
Moraine (LG)
Debris flow cone
Landslide

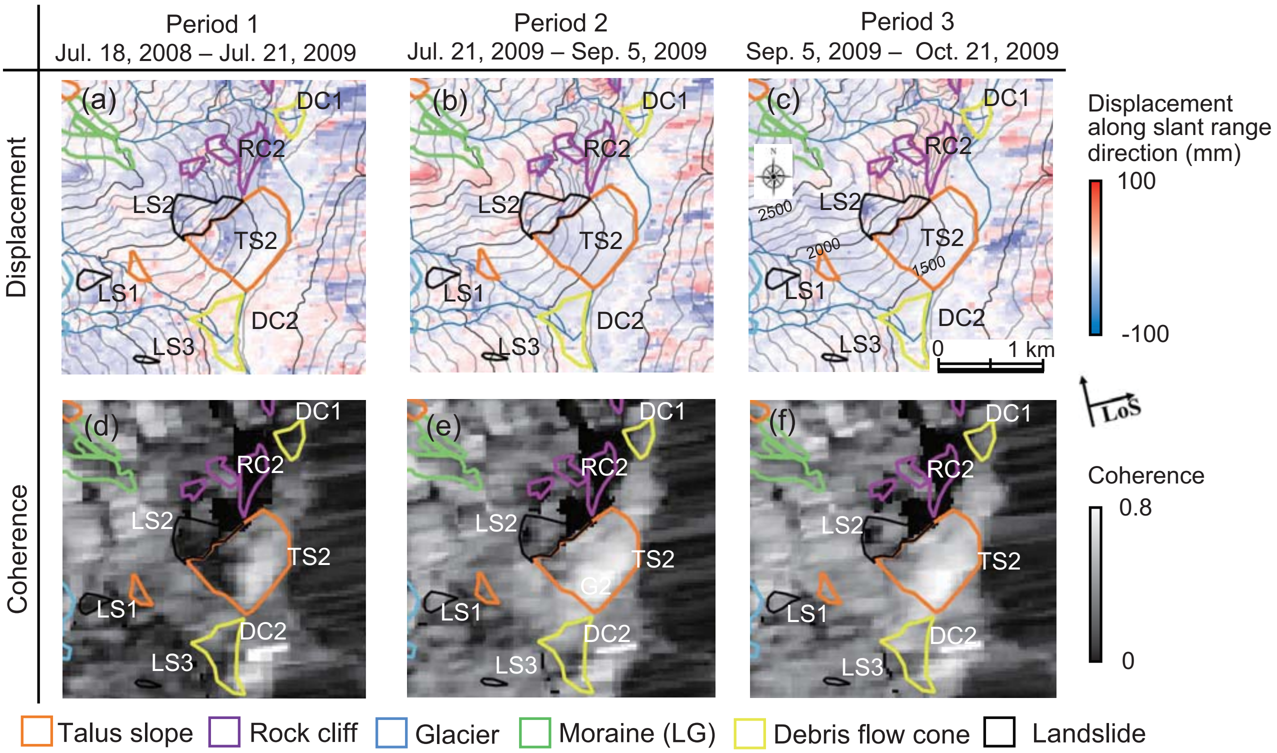
Period 1
Jul. 18, 2008 – Jul. 21, 2009
Period 2
Jul. 21, 2009 – Sep. 5, 2009
Period 3
Sep. 5, 2009 – Oct. 21, 2009
Displacement
Coherence
(a)
(b)
(c)
(d)
(e)
(f)
DC1
RC2
LS2
TS2
LS1
DC2
LS3
G2
2500
2000
1500
0
1 km
Displacement along slant range direction (mm)
100
-100
LoS
Coherence
0.8
0
Talus slope
Rock cliff
Glacier
Moraine (LG)
Debris flow cone
Landslide

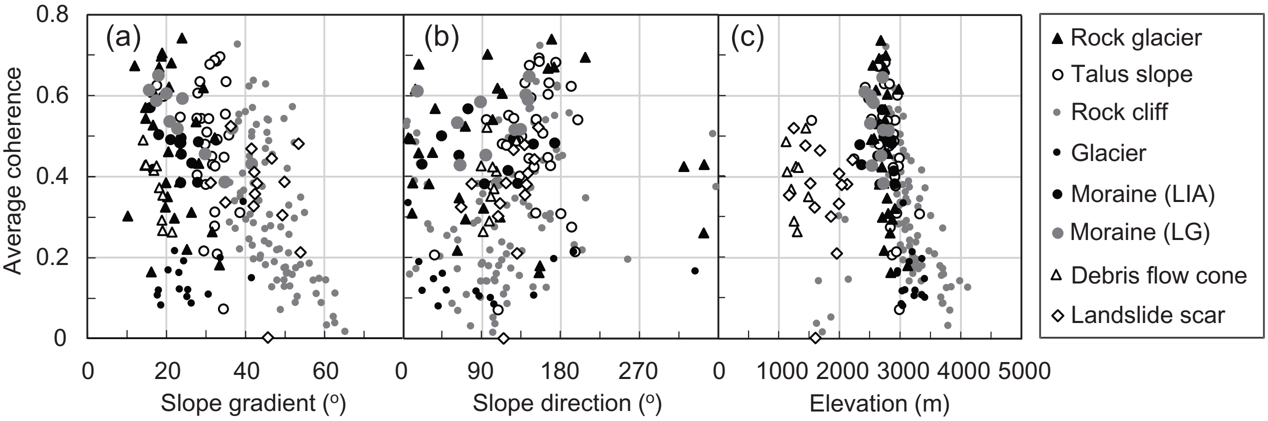
(a)
(b)
(c)
Average coherence
0.8
0.6
0.4
0.2
0
0
20
40
60
Slope gradient (°)
0
90
180
270
Slope direction (°)
0
1000
2000
3000
4000
5000
Elevation (m)
▲ Rock glacier
○ Talus slope
● Rock cliff
● Glacier
● Moraine (LIA)
● Moraine (LG)
△ Debris flow cone
◇ Landslide scar